Pergamon

Journal of Structural Geology, Vol. 19, Nos 3–4, pp. 567 to 581, 1997
© 1997 Elsevier Science Ltd
All rights reserved. Printed in Great Britain
0191–8141/97 $17.00 + 0.00

PII: S0191–8141(96)00097–1

Bedding-plane slip in initial stages of fault-related folding

M. L. COOKE* and D. D. POLLARD

Department of Geological and Environmental Sciences, Stanford University, Stanford, CA 94305-2115, U.S.A.

(*Received* 5 *February* 1996; *accepted in revised form* 21 *October* 1996)

Abstract—Frictional slip along bedding planes contributes to fault-related folding of layered rocks. We use numerical experiments to investigate the deformation of frictional bedding planes near dipping faults under layer-parallel contraction and extension. Within the numerical experiments, contraction boundary conditions produce asymmetric anticlines and extension produces asymmetric synclines. The fold shape may be used to infer dip of the underlying fault in situations where the fault may not be observable. Additionally, sense of slip along bedding planes may indicate proximity to the fault tip. Under uniform remote tectonic strain, fault slip induces deformation in both the hangingwall and the footwall. At depths as shallow as 1 km there is no significant difference between fold amplitudes in the hangingwall and the footwall; this result is contrary to many kinematic models currently in use. Kinematic models of fault-related folds commonly include the development of flat-ramp and flat-ramp-flat fault geometries which may be attributed to initial ramp thrusting and later flat development. Our mechanical models show that fault flats may be produced from fault ramps due to slip along frictional bedding planes near the thrust fault tips. Our numerical experiments also evaluate joint initiation; joints perpendicular to bedding are promoted in extensional environments. We compare the results of the mechanical model to kinematic models of fault-propagation folds and conclude that mechanical models offer important insights to better understand the folding process. © 1997 Elsevier Science Ltd. All rights reserved.

INTRODUCTION

Slip along bedding planes contributes to and is evidence of folding. This so-called flexural slip is manifest either as shear failure (e.g. distributed deformation in shales between stronger sandstone or carbonate units) or as frictional sliding on bedding interfaces between similar lithologies. Deformation mechanisms associated with flexural-slip folding may include frictional slip and/or joint development within flexed beds. Irregularities along bedding planes may act as flaws for joint initiation during flexure. Understanding the deformation of bedding planes during folding promises to lend insight into the mechanisms of flexural-slip folding.

Flexural-slip folding is a major component of the deformational process near faults within contractional and extensional tectonic regimes. Folds have been observed over bends in thrust ramps (fault-bend folds) (Suppe, 1983; Chester *et al.*, 1991; Lewis and Couples, 1993) and above fault terminations such as fault-propagation folds (Suppe and Medwedeff, 1990; Chester *et al.*, 1991) and drape folds (forced folds) (Ameen, 1992; Becker, 1994; Mollema, 1994). Observations from outcrops (Philip and Meghraoui, 1983; Tanner, 1989; Jackson and Pollard, 1990; Ameen, 1992; Becker, 1994), boreholes (Lewis and Couples, 1993), and experiments (Chester *et al.*, 1991) show evidence for bedding-plane slip and demonstrate that flexural slip is integral to the mechanics of folding in some geologic settings.

Co-seismic slip along bedding planes observed within actively deforming folds (Yeats, 1986) confirms the contribution of this mechanism to folding during earthquakes. Flexural slip of up to 1 m was observed associated with the 1980 El Asnam earthquake (Philip and Meghraoui, 1983). Co-seismic slip along folded layers was observed adjacent to the eastern Elmore Ranch Fault in the Superstition Hills earthquake of 1987 (Klinger and Rockwell, 1989). Thus, bedding-plane faults have been shown to contribute to deformation within actively deforming folds and should not be overlooked in the mechanical analysis of ancient folds.

Broadly speaking, the deformation in some folds may be described as 'ductile' and mechanisms such as crystal plasticity provide what appears at the outcrop scale to be a continuous displacement field. The rock units seem to have 'flowed' into their contorted shapes with little or no loss of cohesion or separation. The continuum mechanical theories of plasticity and viscosity have been successfully employed to analyze and explain such folded shapes (Hudleston and Lan, 1994; James and Watkinson, 1994; Johnson and Fletcher, 1994; Erickson and Jamison, 1995). In contrast, the deformation associated with other folds may be described as 'brittle' because mechanisms such as fracture and faulting provide what appears at the outcrop scale to be a discontinuous displacement field. The rock units appear to have been broken into discrete blocks that have moved relative to one another. The continuum theories of elasticity and fracture mechanics offer appropriate tools for analyzing and explaining such folds. Here we use a numerical method, developed to analyze faults, joints,

* Current address: Geological Engineering Program, Department of Geology and Geophysics, University of Wisconsin-Madison, 1215 W. Dayton Str., Madison, WI 53706-1692, U.S.A.

and other displacement discontinuities, to study certain aspects of brittle fault-related folding.

We have performed numerical experiments of flexure initiation near faults within extensional and contractional tectonic regimes. These experiments permit analysis of the interdependence of fold and fault development in early stages of the deformation. The initial fold–fault relationships will likely influence later deformation (Johnson and Fletcher, 1994, p. 247) and thus are a worthy topic for investigation. We have extended a Boundary Element Method (BEM) code to examine flexural-slip deformation and use the results to discuss several current topics in fault-related folding including: development of flats from fault ramps, footwall deformation, fold shapes in extensional regimes, and the contrasting fold shapes of kinematic and mechanical models.

PREVIOUS RESEARCH

Kinematic models of fold development, based on geometrical relationships, have been used to study the temporal evolution of complex fault-related folds. Using concepts of conservation of layer area in cross-section, and conservation of layer length, researchers have proposed geometric constructions for balanced cross-sections (Dahlstrom, 1969; Elliott, 1983). The results of kinematic analyses of fold-and-thrust belts which have undergone multiple phases of deformation have added to our knowledge of the tectonic history of orogenic belts (Price and Mountjoy, 1970; Boyer and Elliott, 1982; Jamison, 1987; McMechan and Thompson, 1989; Suppe and Medwedeff, 1990). However, the limitations of area and bed length conservation in understanding folding are recognized by many researchers. Recent applications of the kinematic models have included special features to examine complexities such as layer thinning (Jamison, 1987; Suppe and Medwedeff, 1990; Mosar and Suppe, 1992), out of plane movement of material (Apotria *et al.*, 1992) and layer-parallel shear strain within layers (Jamison, 1987; Apotria *et al.*, 1992; Mitra, 1992; Mosar and Suppe, 1992). Complexities such as heterogeneous shear strain and layer thinning have been investigated with mechanically-based models using the principles of continuum mechanics (Hudleston and Lan, 1994; Erickson and Jamison, 1995). Mechanical models of fault-related folding are not yet sophisticated enough to reproduce all of the complex deformation within mature fold-and-thrust belts, but they can aid in understanding the mechanics of fold development.

Most studies on mechanics of folding (see reviews and summaries in Johnson and Fletcher, 1994) investigate buckling with the predominant driving stress acting parallel to the layers. However, within fault-associated folds, such as folds above fault tips (Reches and Johnson, 1978; Jamison, 1987; Chester *et al.*, 1991) the predominant flexural forces may not be layer-parallel. If the fault develops prior to folding, the rock will deform in response to both the stress perturbation caused by slip on the fault and layer parallel compression or extension.

Mechanical analysis of folding requires specification of constitutive properties. At depth and under high temperatures rock may deform ductilely and behave as a viscous or plastic material. In contrast, rock within the upper 10 km of the Earth's crust can deform in a brittle manner and behave elastically for relatively small strains and duration of loading (Jaeger and Cook, 1979; Scholz, 1990). We hypothesize that, to first order, the initial formation of some geological folds within the upper crust can be modeled as the flexural deformation of linear elastic layers if one includes the possibility of discontinuities in the displacement field that correspond to structures such as faults, bedding planes and joints or veins. One purpose of this paper is to test this hypothesis by producing models, examining their behavior through parametric analysis, and comparing the results to observations.

The heterogeneous nature of geologic strata can be modeled as layers bounded by interfaces that are weak in shear and tension. Mechanical models show that if layers slip along interfaces when flexed, folds will have greater amplitude and sharper hinges than folds with bonded layer contacts (Chapple and Spang, 1974; Freund, 1979; Koch *et al.*, 1981; Roth *et al.*, 1982). Analytical solutions with zero frictional resistance along bedding planes yield freely-slipping layers which can support no shear stress across interfaces (Reches and Johnson, 1978; Freund, 1979; Koch *et al.*, 1981). Other analytical solutions model interfaces as thin layers with relatively small viscosity (Chapple and Spang, 1974; Pfaff and Johnson, 1989), but incorporating frictional slip along bedding planes is usually too complex for analytical methods. Increasingly complex (and perhaps more realistic) problems can be investigated with numerical models in which the potential for slip can be evaluated anywhere along bedding interfaces and the stress field can be found for any slip configuration. We use a two-dimensional boundary element method to investigate frictional slip and fracture development along bedding interfaces near faults under both layer-parallel contraction and extension.

BOUNDARY ELEMENT METHOD

The Boundary Element Method (BEM) is a numerical technique for solving the governing differential equations of continuum mechanics, including heat and mass transport and solid deformation. In principle, this method can be used to describe the deformation of any solid body if either the tractions or displacements are prescribed along the internal and external boundaries of that body. While other numerical techniques such as the finite element method (FEM) (Zienkiewicz and Taylor, 1989), or the finite difference method (FDM) require meshing of the entire model into discrete elements, the BEM only requires discretization of the internal and

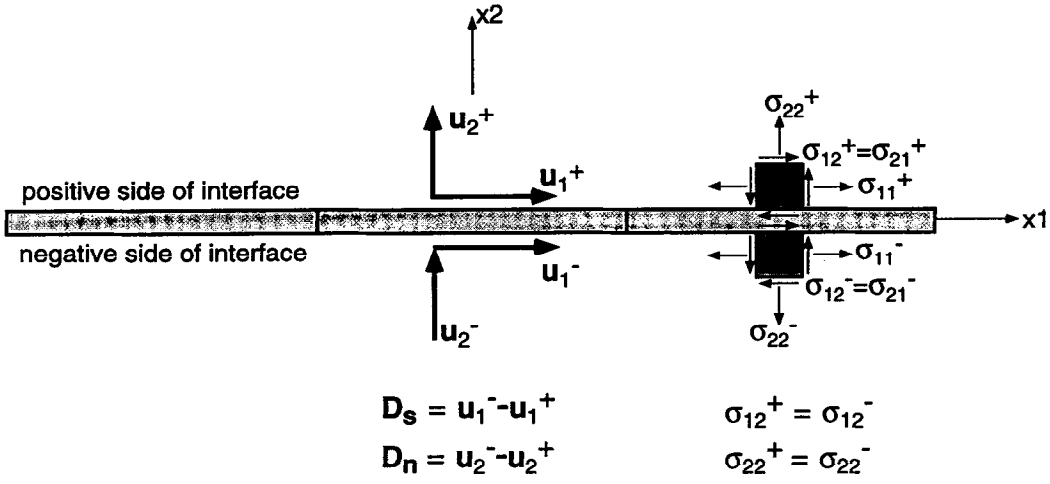

Fig. 1. The shear, D_s, and normal, D_n, displacement discontinuities and stress states on three schematic boundary elements. The displacement discontinuities are defined as the difference in displacement (u_1 and u_2) of the two sides of the interface. Positive D_s values refer to left-lateral shear and negative D_n values refer to opening across the interface. The x_1, x_2 coordinate system is local to each boundary element. Shear stresses, σ_{12}, and stresses normal to element, σ_{22}, are continuous across boundary elements.

external boundaries and interfaces into boundary elements (Crouch and Starfield, 1990; Becker, 1992). The stress, strain, and displacement fields throughout the body are uniquely determined by these boundary conditions

At each boundary element a fundamental solution, for example Kelvin's solution for a line of force integrated along the length of the element (Crouch and Starfield, 1990), is applied that matches the prescribed boundary condition at that element. The mechanical interaction of all the boundary elements is accounted for by solving a system of linear algebraic equations. If tractions are prescribed along a boundary element, for example, the fundamental solution for an element with uniform traction may used to represent that element within this set of algebraic equations. The unknown displacement distribution along the boundary is determined by solving the system of equations. The stress and displacement at any point within the body can be found once the displacements and stresses along the boundaries have been computed.

The two-dimensional BEM code of this investigation uses the displacement discontinuity formulation of Crouch and Starfield (1990). The boundaries are discretized into line elements of equal length, each associated with a normal, D_n, and shear, D_s, displacement discontinuity (Fig. 1). Whether tractions or displacements are prescribed on the elements, the displacement discontinuity is constant along the length of each element. For traction boundary conditions the traction at the center of the element is specified. This formulation of the BEM is adept at capturing the mechanical behavior of cracks, fractures, and faults. Thomas and Pollard (1993) added propagation of opening-mode fractures to the BEM code of Crouch and Starfield (1990). We have extended the code to include frictional interfaces and the initiation of opening-mode fractures from regions of stress concentration along frictional interfaces. We apply the enhanced code to investigate the initial folding of frictional interfaces near faults in brittle sedimentary rocks.

Frictional slip

Special boundary elements that can accommodate inelastic slip have been used to model frictional interfaces (Crouch, 1979; Crouch and Starfield, 1990) including geologic structures such as faults. For example, Schultz and Aydin (1990) have used frictional elements to investigate basin formation near curved faults. Slip along elements is inelastic in the sense that it is not necessarily recovered during unloading, but this slip can be reversed by applying the appropriate combination of shear and normal stresses. Unlike standard boundary elements, which require prescribed loading conditions, these frictional elements require prescription of constitutive behavior. The elemental mechanical behavior is described by 4 parameters: shear stiffness, K_s, normal stiffness, K_n, cohesion, c, and coefficient of friction, μ. These elements are well-suited to model bedding-plane slip in folds. We model each interface as a set of frictional elements and use the Coulomb criterion to determine if interface elements slip. This criterion relates the shear stress required for slip to the frictional resistance, R (Jaeger and Cook, 1979). Slip occurs under compressive (negative) normal stress, σ_{22}, if the magnitude of shear stress, σ_{21}, exceeds the sum of the cohesion, c, and the coefficient of friction, μ, times the normal stress. Thus we restrict the shear stress as follows:

$$\begin{aligned} &\text{if } \sigma_{22} \leq 0, \\ &\text{then } |\sigma_{21}| < R \text{ where } R = c - \mu\sigma_{22} \\ &\text{if } \sigma_{22} > 0, \\ &\text{then } \sigma_{21} = \sigma_{22} = 0. \end{aligned} \tag{3}$$

If the normal stresses are tensile, there is no longer contact across the interface; shear and normal stresses become zero. For compressive normal stresses, if $|\sigma_{21}| \geq R$, the element will slip until the shear stress drops below the frictional resistance of the element. At this stage, the stress state for the entire system must be recalculated because slip on one element may change the normal and shear stresses on neighboring parts of the interface. The shear stress on elements adjacent to the slipped element may then exceed the frictional resistance and slip as well. For example, Fig. 2 schematically shows how shear stresses along a frictional interface may respond to slip on a hypothetical element 'n' through successive iterations. After several iterations, shear stresses on the fault elements approach the frictional resistance, and displacement discontinuities begin to converge to the solution for that loading step.

The solution converges when the relative difference between shear stresses, σ_{21}, of successive iterations, $k-1$ and k, is less than the prescribed tolerance.

$$\text{tolerance} > \frac{|\sigma_{21}^{k}| - |\sigma_{21}^{k-1}|}{1 + |\sigma_{21}^{k-1}|} \tag{2}$$

Equation (2) is a version of the relative difference formulation (Acton, 1990, p. 49) which is capable of quantifying the shear stress differences for values near zero by adding a factor of 1 to each term. For large shear stresses ($\sigma_{21} \gg 1$) the denominator of equation (2) approaches the value of the shear stresses at the previous iteration and the formula calculates the percentage difference of shear stresses between iterations. For small shear stresses ($\sigma_{21} \ll 1$) equation (2) calculates the absolute difference (Acton, 1990, p. 49). If the user prescribes a tolerance of 0.1 then the solution is considered to be converged when the relative difference between successive iterations (equation 2) is less than 0.1. Lower tolerances require more iterations to reach convergence.

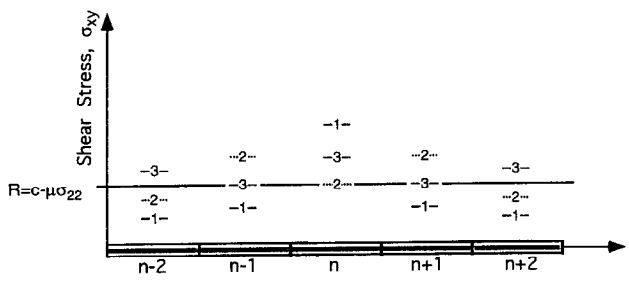

Fig. 2. Schematic convergence of shear stress at the centers of five hypothetical elements with successive iterations. At iteration 1 the shear stress on element n exceeds the frictional resistance, R, and the element is allowed to slip. Here, frictional resistance is defined as the cohesion, c, minus the friction coefficient, μ, times the normal stress. After element n slips the shear stress on n is reduced and the shear stresses on neighboring elements increases. At the second iteration, elements $n-1$ and $n+1$ slip to bring shear stress below the frictional resistance. Iterations proceed in this manner until the solution converges.

To gain experience with frictional elements and to test their usefulness in the analysis of folding, we used frictional elements for preliminary modeling of simple, sinusoidal, two-layer folds. The end-member results ($K_s = 1000$ GPa $\approx \infty$ and $K_s = 0$ GPa) matched those of the analytical solutions for bonded and frictionless interfaces (Cooke, 1994). The success of this test validates the numerical method and encourages us to proceed with the more complex models.

An important constraint on the development of flexural slip is the depth of burial during folding. Since the slip on a frictional interface is related to the normal stresses across it, the weight of sedimentary overburden is a significant deterrent to development of bedding-plane faults at depth. The sedimentary overburden loading is modelled by superposing a constant lithostatic loading. The total stress state at any point is the combined effect of all the active structures (faults, bedding, and/or fractures), tectonic loads (layer-parallel extension or contraction), and lithostatic loads:

$$\begin{aligned} \sigma_{xx} &= \sigma_{xx}(\text{structures}) + \sigma_{xx}(\text{tectonic}) - \rho g d \\ \sigma_{yy} &= \sigma_{yy}(\text{structures}) - \rho g d \\ \sigma_{yx} &= \sigma_{yx}(\text{structures}) \end{aligned} \tag{3}$$

where ρ is the homogeneous rock density, g is acceleration of gravity, and d is the depth, the subscripts x and y refer to the global coordinate system (x—horizontal; y—vertical). The tectonic loading is monotonically increased in order to minimize the path-dependent effects of inelastic frictional slip. We neglect the effect of topography. In general the stresses imposed by topographic variations will only be felt within a region of radius equal to the length scale of these variations (McTigue and Mei, 1981). For our purposes the topographic length scale is postulated to be small compared to the length scale of the active structures.

Joint initiation

Frictional interfaces may act to concentrate stresses and promote joint development. Opening-mode fractures (joints) initiate where the tensile stresses exceed the tensile strength of the rock. Along frictional interfaces, failure of intact rock is determined from the stress state above and below the interfaces (Fig. 1). After the solution has converged for all elements, the maximum tensile stress is determined from the normal (σ_{22}), shear (σ_{12}) and tangential (σ_{11}) stresses above and below each frictional element. While the element shear and normal stresses must be continuous across the interface, the tangential stress may be discontinuous due to slip along the interface. The stress states both above and below the slipping interface are computed as demonstrated in the Appendix. If the maximum tensile stress exceeds the

tensile strength of the rock at any point along the frictional interface, a fracture is added.

The initial angle at which the new fracture grows is determined from the orientation of the maximum tensile stress at the initiation point according to the relationship: opening-mode fractures grow perpendicular to the direction of maximum tension (Jaeger and Cook, 1979; Lawn, 1993). The new fracture orientation is calculated and a new fracture element added to the problem. The new fracture length equals that of the frictional element from which it initiated and the fracture is considered open (no shear or normal stresses on its surfaces). The boundary value problem must be recalculated with the new fracture in place before incrementing the monotonic boundary conditions (tectonic strains).

MODEL DESCRIPTION

We investigate the deformation along initially horizontal, frictional bedding interfaces near dipping faults under applied horizontal contraction and extension. Fold shape will depend on the geometry of the underlying fault, the geometry of the mechanical layering, the proximity of the fold to the Earth's surface and the frictional properties of the bedding surfaces near the fault. We use a simple model in which the contributions of each parameter may be analyzed (Fig. 3).

The lower and side boundaries of the model are chosen far enough away to minimize their influence on the folding deformation above the fault. The top boundary is traction-free, representing the Earth's surface. A tectonic strain is applied to the model by displacing the left boundary horizontally to simulate either contractional or extensional regimes. The horizontal displacement decreases across the 2 km between the left and right sides of the model. The shear stresses on the side and lower boundaries are prescribed to be zero so that these boundaries lie along principal stress directions. The right boundary cannot displace horizontally, nor can the lower boundary displace vertically.

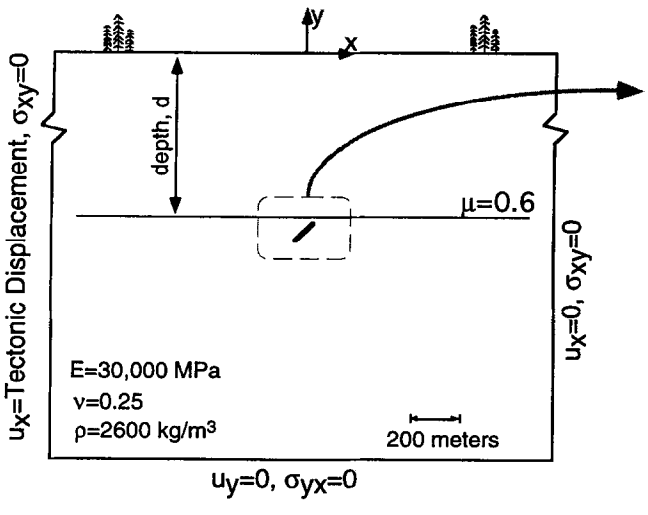

Fig. 3. Configuration of numerical experiments. The top surface of the model represents the traction-free Earth's surface. The depth to frictional interface, d, vertical distance between interface and fault, c, and fault dip, θ, are altered in parametric studies to evaluate the contribution of each to fault-related folding.

Folding is induced within the model by a 100 m long fault. In this model, we use frictional elements to comprise both the fault and the frictional bedding interfaces (Table 1). The fault is compliant in shear ($K_s = 0$) so that any resolved shear stresses acting on the fault plane induce slip. The tectonic layer-parallel contraction promotes slip on the fault which, in turn, promotes flexure of overlying interfaces. To investigate deformation of bedding planes during initial stages of fold development, a frictional interface is placed above and/or below the fault. This interface has very high normal and shear stiffnesses ($K_s = K_n = 1 \times 10^5$ MPa), no cohesion and a friction coefficient, μ, of 0.6. The high normal and shear stiffnesses insure that the element deforms due to Coulomb friction and not elastically. Lithostatic loading is applied to the model with a rock density of 2600 kg m^{-3}. The tolerance for convergence in all cases is 0.001 and takes from 1 to 20 iterations. Constitutive properties are summarized in Table 1.

Within this study we analyze the contributions of 3 parameters to the deformation of frictional interfaces within both extensional and contractional tectonic regimes: depth, fault dip, and distance between the fault and bedding plane. For investigation of deformation within contractional regimes, the left boundary is displaced to the right in increments of 2.5 m. The average horizontal normal strain, ϵ_{xx}(av), imposed on the model is the horizontal displacement at the left boundary, $u_x(x = -1$ km) divided by the total length of the model,

Table 1. Summary of constitutive properties of rock mass, fault, and bedding interfaces as well as prescribed conditions on joints introduced when fracture initiation conditions are met

Rock mass		
Young's Modulus	E	30 GPa
Poisson's ratio	ν	0.25
tensile strength	T	5.0 MPa
Fault	Frictional BEM elements	
shear stiffness	K_s	0
normal stiffness	K_n	1×10^5
cohesion	c	0
friction	μ	0
Bedding interfaces	Frictional BEM elements	
shear stiffness	K_s	1×10^5
normal stiffness	K_n	1×10^5
cohesion	c	0
friction	μ	0.6
Joints	Fracture BEM elements	
shear traction	σ_s	0
normal traction	σ_n	0

2 km; the average horizontal strain increment for each increment of loading is -1.25×10^{-3}. The slip distribution and vertical displacement of the interface (fold shape) are noted. In numerical experiments of extensional deformation the left side of the model is displaced to the left in increments of 0.25 m producing an average horizontal normal strain increment of 1.25×10^{-4} across the model. The left boundary is incrementally displaced for both contraction and extension models until either fractures develop or the strain reaches 1% ($\pm 1 \times 10^{-2}$), here taken as the limit for infinitesimal elastic strain. The horizontal strain increment for extension is an order of magnitude less than that for contraction because less extension is need to initiate fractures than horizontal contraction. The fold shape, slip distribution and fracture pattern along the frictional interface are recorded for each case. The fault dip varies between cases.

CONTRACTIONAL DEFORMATION

The contraction of the model induces reverse slip along the fault and alters the local stress field (Fig. 4a). In the absence of a fault, the maximum principal stress is approximately -25 MPa for a contractional strain of -3.75×10^{-3}. Reverse slip on a 45° dipping fault produces regions of both higher and lower maximum principal stress near the fault tips (Fig. 4a). The maximum principal stresses along horizontal interfaces above and below the thrust fault will be more compressive than -25 MPa in the compressional quadrant of the fault and more tensile than -25 MPa in the tension quadrant of the thrust fault (Fig. 4b).

Influence of vertical distance between interface and fault

Frictional interfaces which lie closer to the fault tip will experience greater deformation than those away from the fault tip. We examine the fold shape and slip distribution along a frictional interface located at different vertical distances and under the conditions listed in Table 2.

At 0.375% contraction the normal stresses acting on the interface 10 m below the fault exceed the tensile strength of the rock between $-55 < x < -40$ m, within the tensile quadrant of the thrust fault. The normal stresses on the interface 10 m below the fault are slightly more tensile than the normal stresses 10 m above the fault because the hanging wall moves farther than the footwall

Table 2. Parameter values used to evaluate the influence of distance between interface and fault on contractional deformation

Parameter		Value
Depth	d	1 km
Vertical distance	c	10, 25 and 50 m
Fault dip	θ	45°
Average strain	ϵ_{xx}(av)	-3.75×10^{-3}

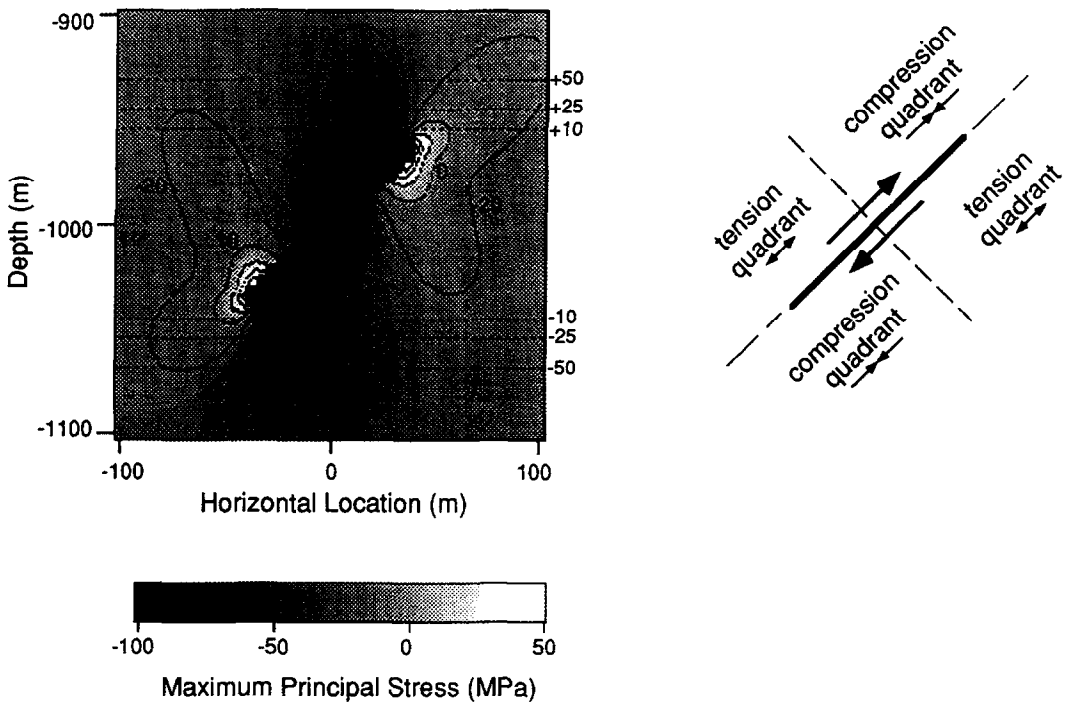

Fig. 4. (a) Maximum principal stresses around a 45° dipping fault under horizontal contractional strain of -3.75×10^{-3}. The maximum principal stress increases near the fault tips. The horizontal lines indicate locations of frictional interfaces that will be studied in the contractional parametric studies. (b) The fault slips in a right-lateral sense producing relative tension in the upper right and lower left regions (quadrants) of the fault and increased compression in the upper left and lower right regions of the fault.

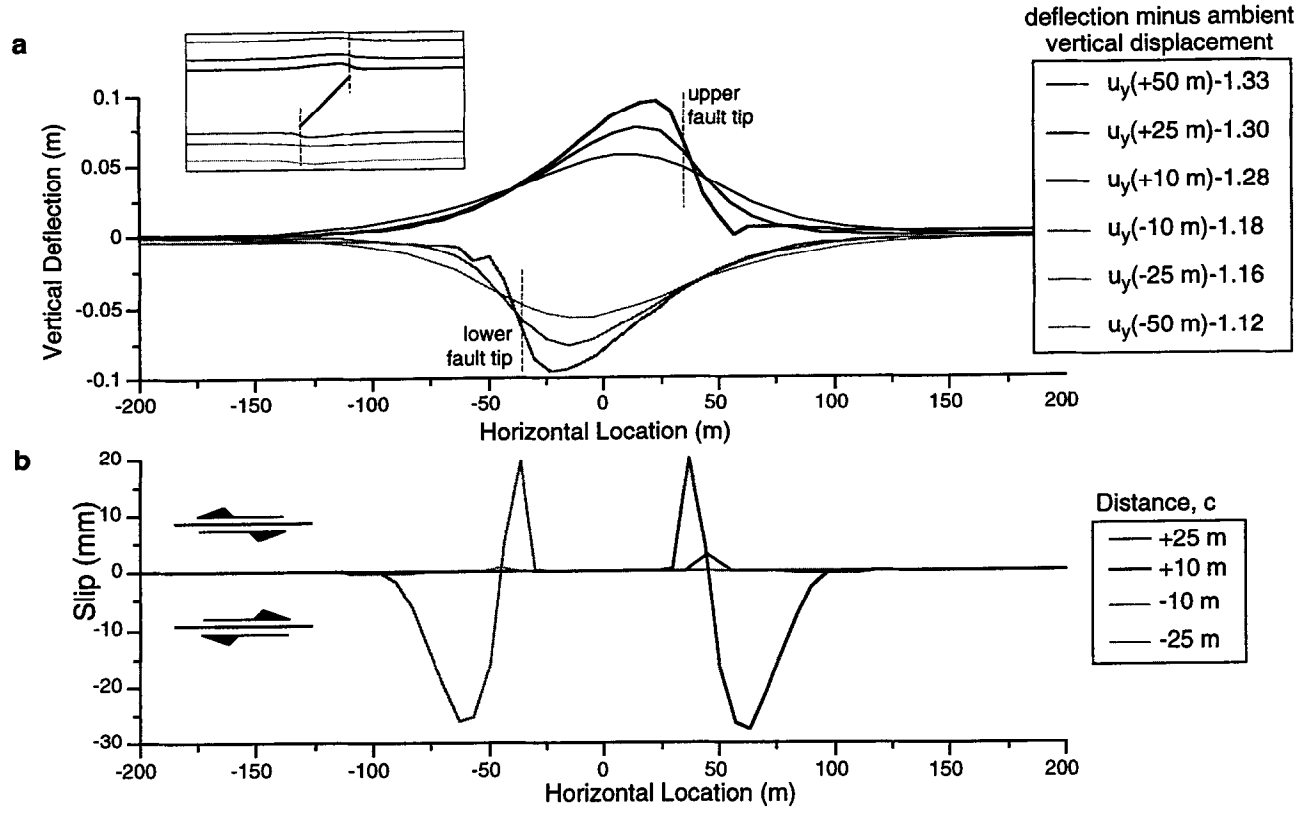

Fig. 5. (a) Vertical deflection along frictional interfaces above and below 45° fault. Deflections along +10, +25, and +50 refer to interfaces 10, 25, and 50 m above the upper fault tip and deflection along −10, −25, and −50 refer to interfaces 10, 25, and 50 m below the lower fault tip. Each deflection curve expresses the deflection of the interface minus the ambient vertical displacement. The location of the upper and lower fault tips are indicated with light dotted lines. Fold amplitude and asymmetry decrease with distance from the fault tip. (b) Slip along frictional interfaces above and below a 45° fault. Left-lateral slip is positive and arrows on the figure show direction of relative slip. Slip magnitude increases with distance to fault tips. Left-lateral slip corresponds to flexural slip within the folds while right-lateral slip does not. The regions of right-lateral slip lie ahead of the right-lateral dipping fault and act to extend the length of the fault.

resulting in larger tensile stresses near the lower fault tip. The traction-free surface at the top of the model, which represents the Earth's surface, allows the hanging wall of the fault to be displaced more than the footwall. Since the tensile strength is exceeded within the model, fractures initiate parallel to bedding in the rock adjacent to the interface at -3.75×10^{-3} strain and no further strain increments are applied.

The region above the fault flexes into an asymmetric anticline with a steep right limb while the region below the fault deforms into an asymmetric syncline with a steep left limb (Fig. 5a). The interfaces closer to the fault tips have greater fold amplitude, steeper limbs and smaller fold lengths than those farther from the fault. Fold asymmetry of a flexed interface decreases with distance from the fault.

Since the entire model is displaced upward in response to horizontal contraction, the amount of vertical displacement depends on the depth within the model. The ambient vertical displacement decreases with depth to zero at the lower boundary. In the region of the fault, all of the material is displaced upward over 1 m. Each deflection curve represents the vertical displacement of the interface minus the ambient vertical displacement determined from a model with neither faults nor frictional interfaces (Fig. 5a).

Slip along horizontal frictional interfaces decreases with vertical distance to the fault (Fig. 5b). At contractional strain of -3.75×10^{-3}, shear stresses along the interfaces 50 m above and below the fault are not great enough to produce frictional slip. The interfaces 25 m above and below the fault slip left-laterally along the steep right-dipping limbs of the anticline and syncline. This sense of slip corresponds with that expected in flexural-slip folds; the upper layer moves toward the anticlinal hinge. Within this paper we use the terms right- and left-lateral to describe the sense of slip; we do not intend to suggest strike-slip movement on the bedding interfaces. The shear stresses along the shallower left-dipping limbs of the anticline and syncline are not great enough to produce slip on these interfaces at this strain. The interface 25 m above the fault has a greater slip magnitude than the interface 25 m below the fault because the lithostatic stresses which inhibit frictional slip are less at shallower depths.

The slip along the interfaces 10 m above and below the fault is greater than that for the interfaces 25 m from the fault. Left-lateral offset corresponding to flexural slip

occurs along the right-dipping limbs of the anticline and syncline near the fold hinges. However, most of the slipping interface elements experience right-lateral offset along the right-dipping limbs of the folds. This right-lateral slip along frictional layers results from the right-lateral shear stress induced on the interface by reverse slip on the dipping fault. At some distance from the fault the interface deformation is predominantly flexural ($x = \pm 25$ m, Fig. 5b), but near the fault tip the local stress field dominates interface deformation ($x = \pm 10$ m, Fig. 5b). In field observations, sense of bedding-plane slip that does not correspond to flexural slip may be a diagnostic feature for inferring the presence and slip on an unexposed fault.

Influence of fault dip

Deformation along the frictional interfaces will depend on fault dip. We examine the fold shapes along the frictional interfaces under conditions described in Table 3 to determine the role of fault dip. In the rest of the parametric studies presented in this paper we only examine deformation above the fault. The region below the faults for all of the studies in this paper deforms in the manner described above.

Table 3. Parameter values used to evaluate the influence of fault dip on contractional deformation

Parameter		Value
Depth	d	1 km
Vertical distance	c	10 m above fault
Fault dip	θ	15°, 30°, 45°, 60°, and 75°
Average strain	ϵ_{xx}(av)	-3.75×10^{-3}

At 0.375% contraction the normal stresses acting across the interfaces above the 45° and 60° dipping faults exceeds the tensile strength, and strain incrementation is stopped. All vertical deflection profiles in Fig. 6(a) show deformation at 0.375% contraction. The largest amplitude fold occurs above the 45° fault with decreasing amplitude folds over steeper and shallower faults (Fig. 6a). Because the faults are prescribed to have zero shear stiffness ($K_s = 0$) and zero friction ($\mu = 0$), the 45° dipping fault with the greatest resolved shear acting upon it due to the prescribed horizontal contraction has the greatest slip. As the fault dip increases, the fold hinge moves to the left (down-dip direction for the fault). The fold shapes are asymmetric in all cases and are dominated by an asymmetric anticline with steeply dipping right limb. For fault dips of $\theta = 15°$ and 30°, there is a small syncline on the back-limb of the anticline whereas fault dips of

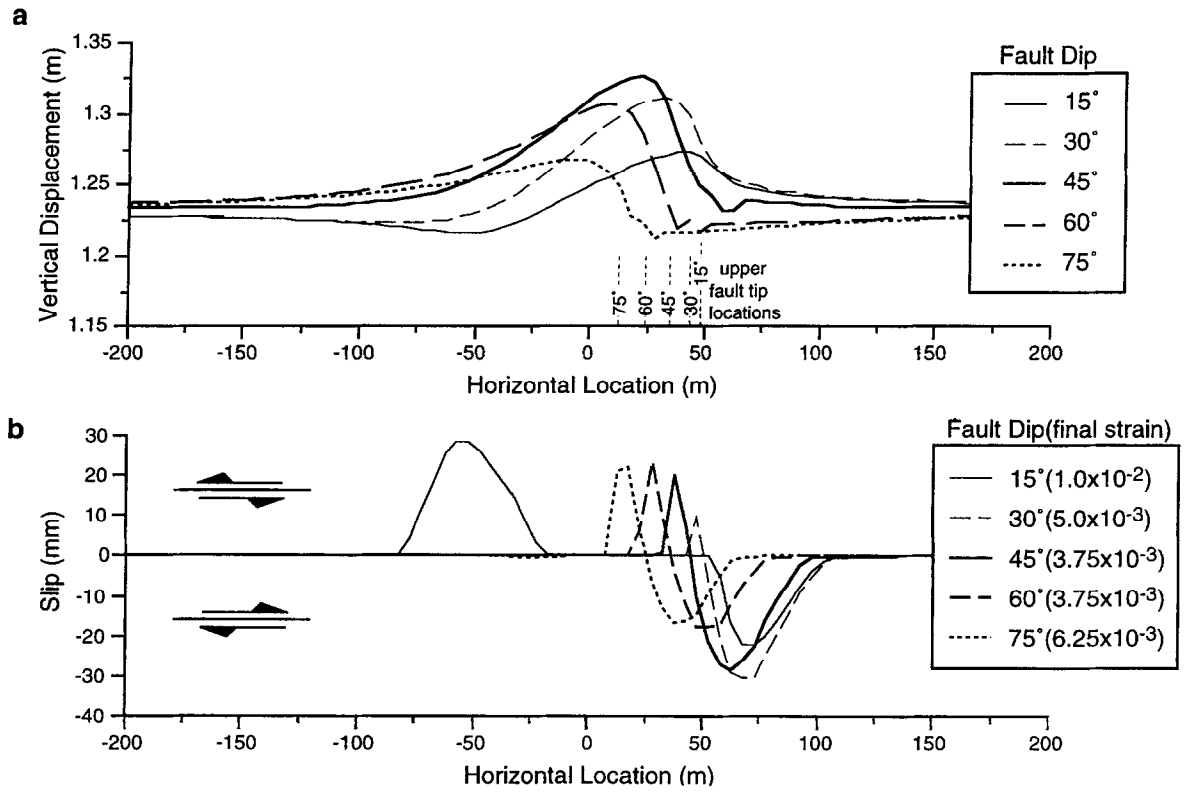

Fig. 6. (a) Vertical deflection of frictional interface 10 m above faults with different dips. The fault depth is 1 km and the strain -3.75×10^{-3}. The 45° dipping fault has the greater fold amplitude. The upper fault tip locations are shown in light dotted lines. As the fault steepens the fold hinge moves toward to fault center (to left) along with fault tip. Small synclines develop on the back limb of the fold for shallow faults (15° and 30° dips) and on the fore limb of the fold for steep faults (60° and 75°). (b) Slip along interfaces above faults of different dips. The final applied strains for each fault are listed in the legend. Both right- and left-lateral slip occur on the frictional interfaces. The right-lateral slip magnitudes are greater than left-lateral for all faults except the 15° dipping fault.

Table 4. Limiting strain and location of bedding parallel fractures for different fault dips

Fault dip	Strain	Location of fractures
15°	-1.0×10^{-2}	none
30°	-5.0×10^{-3}	$50<x<60$ m
45°	-3.75×10^{-3}	$40<x<55$ m
60°	-3.75×10^{-3}	$25<x<35$ m
75°	-6.25×10^{-3}	$15<x<30$ m

Table 5. Parameter values used to evaluate the influence of burial depth on contractional deformation

Parameter		Value
Depth	d	0.5, 1, and 2 km
Vertical distance	c	10 m above fault
Fault dip	θ	45°
Average strain	ϵ_{xx}(av)	-2.5×10^{-3}

$\theta=60°$ and 75° produce a small syncline to the right of the forelimb. The syncline amplitudes are greatest for the 15° and 75° dipping faults.

Contraction of the models with different fault dips continues until either fractures develop or the strain reaches 1%. The final strain differs for the tested fault angles (Table 4 and Fig. 6b). Faults dipping 45° and 60° require the least contractional strain to produce fractures while the 15° dipping fault does not produce fractures before the average strain reaches the prescribed elastic limit. Fractures develop within the tensile quadrant of the thrust fault. For shallow faults the horizontal interfaces lies primarily within the compressional quadrant of the fault where fracture initiation is inhibited. Table 4 shows how the location of bedding-parallel fractures moves towards the fault center as the fault dip steepens.

The slip distributions on the interface show both a right-lateral and left-lateral sense of slip (Fig. 6b). The regions of left-lateral slip for all but the 15° dip correspond to flexural slip along the right-dipping limb of the anticlines. There is a sharp transition from left- to right-lateral slip for these faults. For the 15° dipping fault, the right dipping limb of the anticline does not experience flexural slip rather, there is a broad syncline to the left of the anticline and left-lateral slip develops on both limbs of that syncline. The regions of right-lateral slip occur above and to the right of all fault tips. This sense of slip along the interface is induced by reverse slip on the fault.

Influence of depth

The nature of deformation along frictional interfaces will depend on depth. Increasing depth increases the compressive stress acting across the horizontal interfaces and thereby inhibits frictional sliding. We investigate the deformation along a frictional interface at different depths under the conditions listed in Table 5.

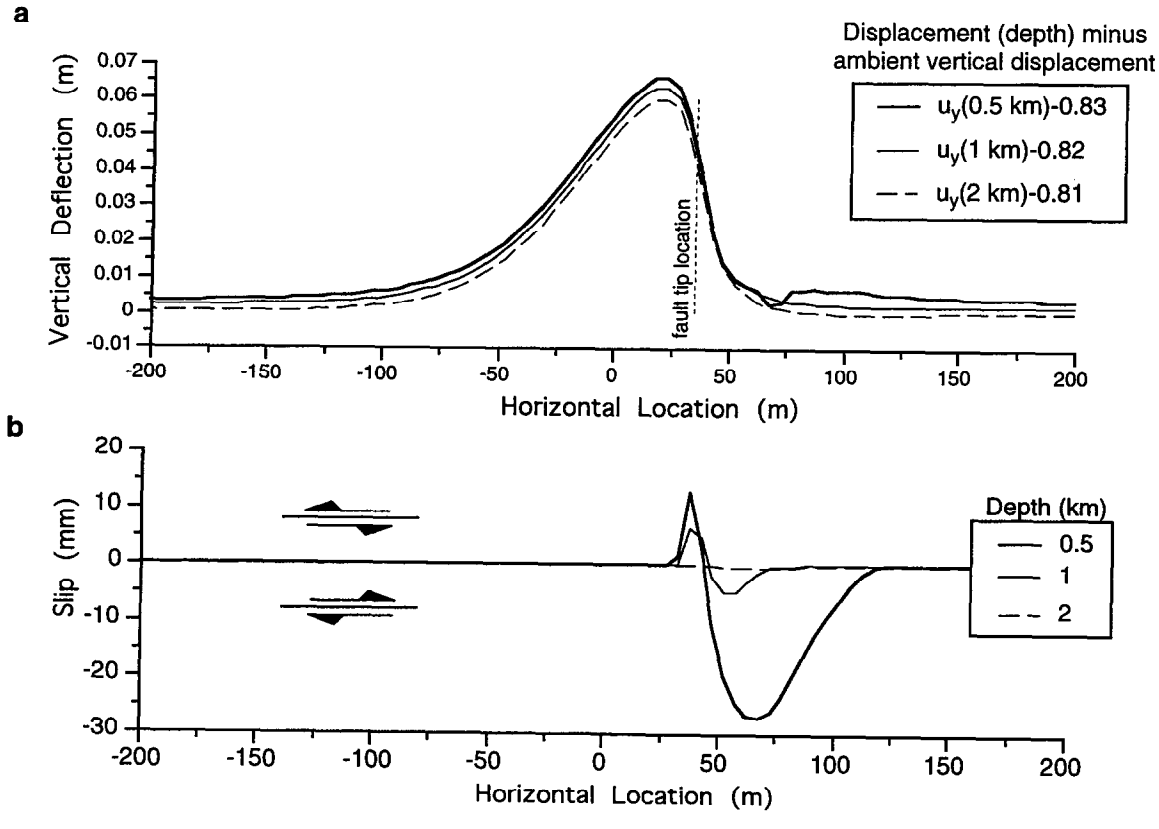

Fig. 7. (a) Vertical deflection of frictional interface at different depths above a 45° fault for strain of -2.5×10^{-3}. The fold shapes are similar but the shallower interfaces have greater fold amplitude. (b) Slip distributions along the interface at different depths. Slip increases with decreasing depth due to decreased lithostatic loads.

At 0.25% contraction the tensile stresses acting on the interface at a depth of 0.5 km exceed the tensile strength of the rock producing bedding parallel fractures between $40 < x < 65$ m. The vertical deflections along interfaces at depths of 0.5, 1, and 2 km in Fig. 7(a) and the slip distributions in Fig. 7(b) are for an average strain of -2.5×10^{-3}.

The anticlinal fold shapes are similar for faults at these three depths. All have a comparable amplitude and are asymmetric with a steep right-dipping limb (Fig. 7a). Deflection curves are normalized by subtracting the ambient vertical displacement determined from models without faults or interfaces. Since the ambient vertical deflection due to horizontal contraction of the model decreases with depth, shallower interfaces are subjected to greater ambient vertical displacement (Fig. 7a, legend). The greatest magnitude of deflection occurs at the shallowest depths where slip is promoted by lower lithostatic loads.

While the fold shapes at different depths do not vary greatly, the bedding-plane slip distributions in the folds are different for each of the depths investigated (Fig. 7b). Slip is greater for the shallower fault. For a strain of -2.5×10^{-3} there is no slip on an interface buried 2 km. At 1 km and 0.5 km depths there is both left and right-lateral slip on the right dipping limb of the fold. The left-lateral slip along the right-dipping limb of the anticline is consistent with the flexural deformation whereas right-lateral slip is induced by the thrust fault.

EXTENSIONAL DEFORMATION

Layer-parallel extension promotes bedding-perpendicular joint growth. When the model extends in the absence of a fault to a strain of 1×10^{-3}, the tensile stress, σ_{xx}, everywhere in the model is greater than the rock's tensile strength. Opening-mode fractures propagate perpendicular to the maximum tension direction and therefore are bedding-perpendicular. In the absence of a fault, the maximum principal stress is approximately -1.5 MPa for an extensional strain of 7.5×10^{-4}. Tectonic extension of the model drives normal slip along the 45° dipping fault producing local stress concentrations near the fault tips (Fig. 8a). Horizontal interfaces above the fault lie predominantly within the tensional quadrant of the fault (Fig. 8b); greater tension will promote interface slip and initiation of opening-mode fractures.

Influence of fault dip

We examine the fold shape along frictional interfaces under the conditions listed in Table 6 for different fault dips.

All of the faults produce an asymmetric synclinal fold with a steeper left-dipping limb (Fig. 9a). For each dipping fault, the location of the synclinal trough lies above the tip of the fault. The 45° fault produces a single syncline while steeper and shallower faults produce small anticlines to either side of the larger syncline. Anticlines occur up dip of the fault for steep faults and increases amplitude with dip. Anticlines occur down dip of the fault for shallow faults and decrease amplitude with dip.

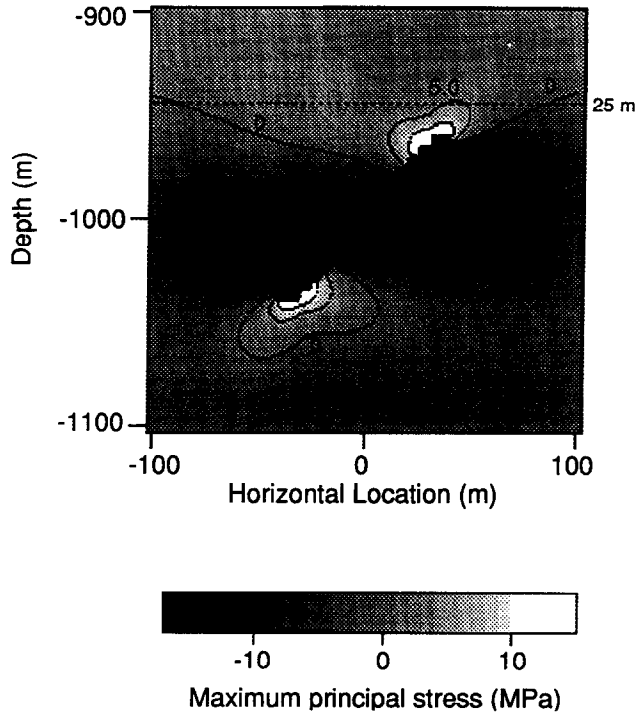

Fig. 8. Maximum principal stress around a 45° dipping fault under horizontal extension. The upper left and lower right quadrants of the fault concentrate tensile stresses while compression is concentrated in the upper right and lower left quadrants. The horizontal line indicates the location of frictional interface analyzed in the extension study.

Within 200 m to either side of the fault center there is a local resultant 'throw' along the interface. For faults steeper than 45° the footwall side of the fold is higher than the hanging wall side. This agrees with the normal fault motion on the underlying fault which lowers the hanging wall relative to the footwall (Fig. 9b). However, the shallow faults (15° and 30°) produce folds whose hanging wall portions are slightly higher than their footwall portions. This local throw may be induced by the proximity of the fault's lower tip to the flexed interface (Fig. 9c). Within the compressional quadrant of the fault there is fault-parallel contraction and some fault-perpendicular expansion which locally uplifts the overlying interface. Longer normal faults will likely produce less hanging wall uplift than shorter faults because the lower fault tip is further from the flexed

Table 6. Parameter values used to evaluate the influence of fault

Parameter		Value
Depth	d	1 km
Vertical distance	c	25 m above fault
Fault dip	θ	15°, 30°, 45°, 60°, and 75°
Average strain	ϵ_{xx}(av)	8.75×10^{-4}

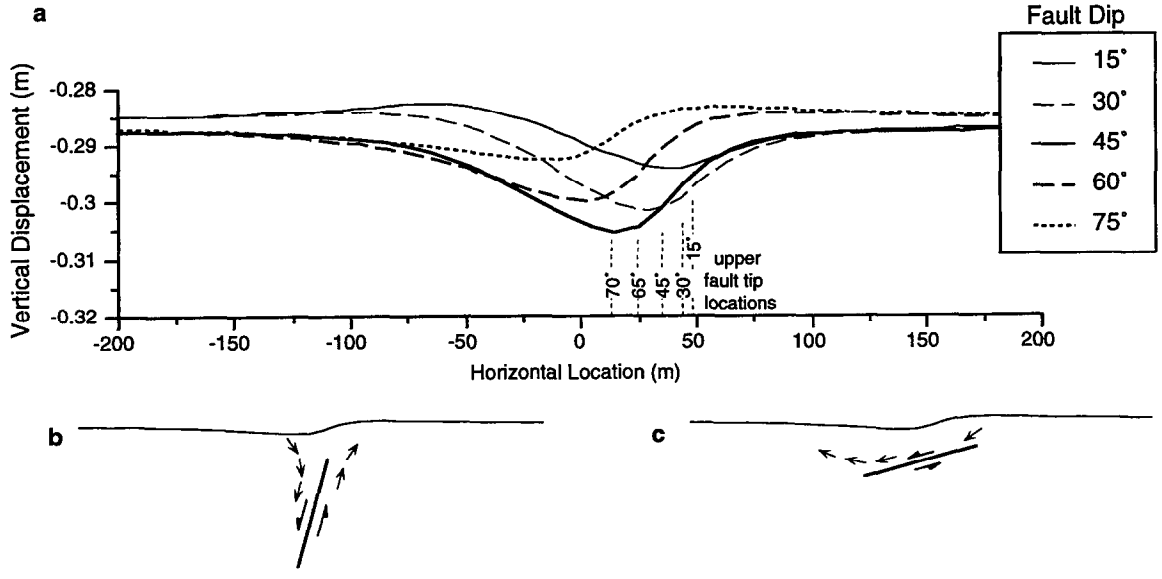

Fig. 9. (a) Vertical deflection of interfaces 25 m above faults under an extensional strain of 8.75×10^{-4}. The fold shape depends on fault dip. The upper fault tip locations are indicated with fine dotted lines. As the fault steepens the upper fault tip and the syncline hinge move towards the fault center (to left on figure). The steep faults (60° and 75°) develop small anticlines to the right of the assymetric syncline whereas the shallow faults (30° and 15°) develop small anticlines to the left of the larger syncline. Within 200 m to either side of the fault center, some faults produce a local 'throw'. (b) Steep faults produce local throws which correspond with slip on the normal fault. Small arrows indicate relative displacement of the material around the fault. (c) For shallower faults (15° and 30°) the bottom tip of the thrust fault influences deformation of the interface producing a fold whose hanging wall portion is slightly *higher* than its footwall portion.

interface. The resultant throw across the folds decreases to zero far away from the fault.

None of the frictional interface elements slip at this level of strain, but fractures develop along interfaces above 15°, 30°, 45°, and 60° dipping faults. Fractures do not develop above the 75° dipping fault before average horizontal strains reach the elastic limit of 1×10^{-3}. This strain is the limiting case for which joints develop everywhere. Above other faults the fractures develop locally along the interface at an average strain of 8.75×10^{-4} (Fig. 10). The fractures develop within the tensional quadrant of the fault. As fault dip shallows from 75° to 45° and steepens from 15° to 45° the region of fracturing widens. For all cases of different fault dips, the fracture orientation varies from 90° to 83° to bedding. The maximum principal stresses exceeds the tensile strength of the rock everywhere within the regions delineated for jointing on Fig. 10.

DISCUSSION

Initial fold shapes

The numerical method used in this mechanical study is best suited to investigate the initial conditions of fold development over a thrust fault ramp. The initial deformation patterns will become amplified during further contraction/extension to produce mature folds (Johnson and Fletcher, 1994, p. 247). We expect that mature folds will share some of the relationships between fold form and the parameters of fault dip, depth and distance to fault with the young folds illustrated in this research. However, many mature fault-related folds contain more complex fault geometries than the single thrust fault ramp investigated in this study (Price and Mountjoy, 1970; Boyer and Elliott, 1982; McMechan and Thompson, 1989). The mature shapes of these folds may be influenced by migration of material through fold hinges.

We have shown that dip of fault ramps controls the shape of folding in the early stage of development. The influence of fault dip on fold shape has also been shown by kinematic models (Jamison, 1987; Chester and Chester, 1990; Suppe and Medwedeff, 1990) and laboratory experiments (Withjack *et al.*, 1990). However, while some kinematic models constrain constant interlimb angle along the fold hinge (kink band) (Suppe and Medwedeff, 1990), the mechanical experiments performed in this study show that fold tightness decreases (wider interlimb angle) with distance away from fault tips. Laboratory experiments on extensional forced folding also show decreased fold tightness away from the fault tip (Withjack *et al.*, 1990). Fold shapes of kinematic models are similar while these numerical mechanical experiments show decreasing fold amplitude away from the fault tip. This mechanical study also shows that fold amplitudes decrease with depth due the contribution of increased lithostatic loading to frictional resistance.

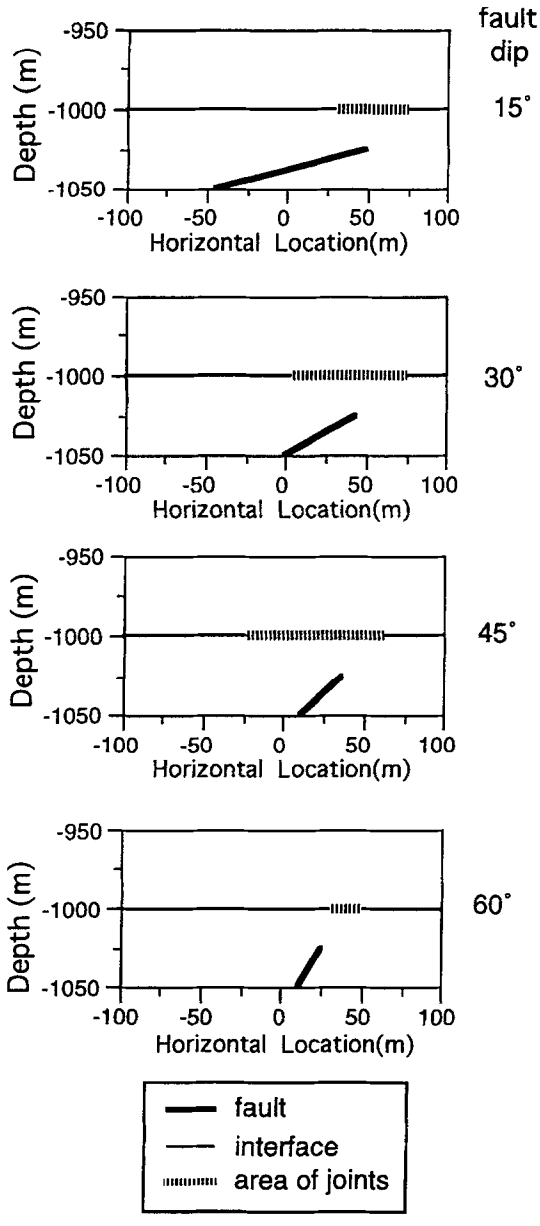

Fig. 10. Location of bedding-perpendicular joints along interfaces 25 m above upper fault tips for faults dipping 15°, 30°, 45° and 60°. The applied extensional strain is 8.75×10^{-4}. No joints develop along the interface above the 75° fault for this strain. The region of jointing is widest for the 45° dipping fault and decreases for shallower and steeper faults.

Development of flats from fault ramps

The mechanical development of fault ramps and flats is not well understood. Many studies of fault related folding either start their investigations with a flat-ramp or flat-ramp-flat structure (Chester and Chester, 1990; Chester *et al.*, 1991), or suggest that ramps develop from the basal flat (Suppe, 1985). Recent investigations of displacement profiles along some flat-ramp-flat thrust faults suggest that these faults initiate as ramps (dipping thrust faults) which cut across layers (Chapman and Williams, 1984; Kattenhorn and McConnell, 1994). Thus ramps may develop first and layer-parallel flats may form later from the fault tips (Eisenstadt and DePaor, 1987). An unresolved problem is how ramp thrust faults propagate along two layer-parallel décollements forming the traditional flat-ramp-flat geometry.

Our analysis of slip along frictional interfaces above and below steeply dipping faults driven by horizontal contraction presents a mechanism for the growth of flats from fault ramps (Fig. 11). The normal stresses across bedding planes within tensional quadrants of the fault are reduced and thereby frictional slip is promoted. The portion of bedding planes ahead of ramps will slip in the same sense as the ramp thus acting to 'extend' the fault length. In addition, slip weakening along the sliding bedding planes may lower friction and encourage the growth of the fault along bedding. Thus, bedding planes near ramp terminations act as weak interfaces onto which the ramp can develop into a ramp-flat geometry. We would expect the potential development of ramp-flat geometry within rock strata at every frictionally weak bedding-plane in proximity of a thrust fault tip.

When propagating towards a frictional bedding plane, the thrust ramp may either deflect along the bedding-plane and form a ramp-flat geometry or it may cross the bedding-plane and continue the ramp geometry. Field evidence shows that ramps commonly cross-cut bedding along which they might have slipped (Suppe, 1985; Ramsay and Huber, 1987) In a given case it may take more or less energy for a thrust ramp to deflect along a pre-existing bedding-plane than to cross the bedding-plane and fracture intact rock. We suggest that the relative energy and conditions for ramp crossing frictional layers should be studied using numerical tools such as presented in this study.

Contractional versus extensional tectonics

The extensional and contractional fold shapes produced in the numerical experiments differ from each other. In contractional tectonic regimes we expect to find anticlines with asymmetry indicating the direction of faulting (vergence). The shallow limb dips in the same direction as the fault (Fig. 6). This result agrees with kinematic models of fault-propagation folds which show that the fore limb is steeper than the back-limb (Chester and Chester, 1990; Suppe and Medwedeff, 1990) Our mechanical results agree with kinematic models which show that fold tightness (inter-limb angle) is an expression of fault dip (Suppe and Medwedeff, 1990).

However, our conclusions for contractional folds above faults differ from kinematic results for fault-propagation folds on some points. Kinematic models do not produce small synclines ahead of the fore limb nor on the back limb. The mechanical numerical experiments do produce small synclines which appear on the fore limb of steep faults (> 45°) and on the back limb of shallow faults (<45°). These results suggest that fault dip may be estimated by the presence and relative location of such synclines.

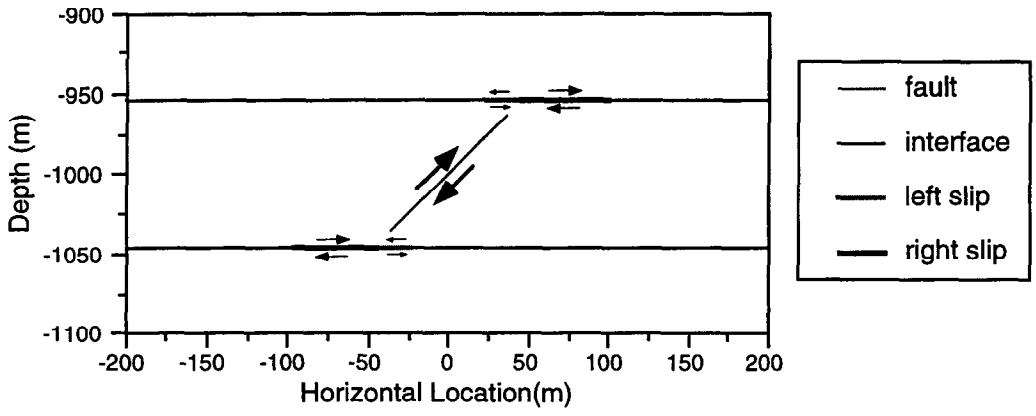

Fig. 11. Geometry of slip along interfaces 10 m above and below a 45° dipping fault. Size of arrows indicates relative slip magnitudes. Regions of the interface just ahead of the fault have the same sense of slip as the fault (right-lateral). This slip is a response of the frictional interface to slip on the fault and acts to 'extend' the fault length. The presence of frictionally weak bedding planes may encourage dipping faults to deflect along bedding and produce ramp-flat fault geometries.

In extensional tectonic regimes we expect asymmetric synclines (Fig. 9). The steepest limb of the fold dips in the same direction as the fault within extensional regimes. These results agree with experimental folding of clay layers over normal faults (Withjack *et al.*, 1990; Mitra and Islam, 1994).

Footwall deformation

Standard kinematic and mechanical studies of folds associated with thrust faults do not allow footwall deformation (Berger and Johnson, 1982; Suppe, 1983; Suppe and Medwedeff, 1990). However, field examples of folds associated with thrust ramps show abundant evidence of footwall deformation and folding (Ramsay and Huber, 1987; Watkinson, 1993; Kattenhorn, 1994). Some kinematic models have produced footwall synclines by allowing thrust faults to break through pre-existing folds (Suppe and Medwedeff, 1990; Fischer *et al.*, 1992) or by applying heterogeneous shear strain near the thrust fault tip (Erslev, 1991). Additionally, drag folding has been suggested as a method of producing footwall deformation (Ramsay and Huber, 1987). All of these mechanisms predict a lower amplitude fold in the footwall than the hanging wall.

Mechanical models of fault-related folding that do not constrain the footwall to be rigid (Fig. 5) suggest that the footwall deforms nearly as much as the hanging wall (Kilsdonk and Fletcher, 1989). Within our numerical models, at a depth of 1 km the amplitude of folds below the fault were not significantly reduced in amplitude relative to those above the fault (Fig. 5). Our mechanical models suggest that one should expect footwall folding associated with faulting within the upper crust of the Earth.

Acknowledgements—This work was funded by DOE grant DE-FG03-94ER14462-A001. We thank David Anastasio, Eric Erslev and Donald Fisher for organizing the 1995 Penrose conference on fault-related folding. The motivation for this work and many of the ideas presented here are derived from that conference. Conversations with Juliet Crider and Simon Kattenhorn and many of the participants of the Penrose Conference challenged my thinking about folding mechanics and offered me new insights into fault-related folding. Lisa Koenig aided in testing of the boundary element code used in this study. This manuscript was greatly improved by comments and suggestions of Martha Withjack, Peter Huddleston and Eric Erslev.

REFERENCES

Acton, F. S. (1990) *Numerical Methods That Work*. The Mathematical Association of America, Washington, DC.

Ameen, M. S. (1992) Strain pattern in the Purbeck-Isle of Wight Monocline: A case study of folding due to dip-slip fault in the basement. In *Basement Tectonics 8: Characterization and Comparison of Ancient and Mesozoic Continental Margins*, eds K. J. Bartholomew, D. W. Hyndman, D. W. Mogk and R. Mason, pp. 559–578. Kluwer Academic Publishers, Butte, Montana.

Apotria, T. G., Snedden, W. T., Spang, J. and Wiltschko, D. V. (1992) Kinematic models of deformation at an oblique ramp. In *Thrust Tectonics*, ed. K. R. McClay, pp. 141–154. Chapman and Hall, London.

Becker, A. (1994) Bedding-plane slip over a pre-existing fault, an example: the Ramon Fault, Israel. *Tectonophysics* **230**, 91–104.

Becker, A. A. (1992) *The Boundary Element Method in Engineering*. McGraw-Hill, Cambridge.

Berger, P. and Johnson, A. M. (1982) Folding of passive layers and forms of minor structures near terminations of blind thrust faults; application to the central Appalachian blind thrust. *Journal of Structural Geology* **4**, 343–353.

Boyer, S. E. and Elliott, D. (1982) Thrust systems. *American Association of Petroleum Geologists Bulletin* **66**, 1196–1230.

Chapman, T. J. and Williams, G. D. (1984) Displacement-distance methods in the analysis of fold-thrust structures and linked fault systems. *Journal of the Geological Society of London* **141**, 121–128.

Chapple, W. M. and Spang, J. H. (1974) Significance of layer-parallel slip during folding of layered sedimentary rocks. *Geological Society of America Bulletin* **85**, 1523–1534.

Chester, J. S. and Chester, F. M. (1990) Fault-propagation folds above thrusts with constant dip. *Journal of Structural Geology* **12**, 903–910.

Chester, J. S., Logan, J. M. and Spang, J. H. (1991) Influence of layering and boundary conditions on fault-bend and fault-propagation folding. *Geological Society of America Bulletin* **103**, 1059–1072.

Cooke, M. L. (1994) Development of bedding-plane faults and fracture localization in a flexed multilyer: A numerical model. In *First North American Rock Mechanics Symposium*, ed. N. A. Laubach, pp. 131–138. Balkema, Austin, Texas.

Crouch, S. L. (1979) Computer simulation of mining in faulted ground. *Journal of the South African Institute of Mining and Metallurgy* **79**, 159–173.

Crouch, S. L. and Starfield, A. M. (1990) *Boundary Element Methods in Solid Mechanics*. Unwin Hyman, Boston.

Dahlstrom, C. D. A. (1969) Balanced cross sections. *Canadian Journal of Earth Sciences* **6**, 743–757.
Eisenstadt, G. and DePaor, D. G. (1987) Alternative model of thrust-fault propagation. *Geology* **17**, 630–633.
Elliott, D. (1983) The construction of balanced cross-sections. *Journal of Structural Geology* **5**, 101.
Erickson, S. G. and Jamison, W. R. (1995) Viscous-plastic finite-element models of fault-bend folds. *Journal of Structural Geology* **17**, 561–573.
Erslev, E. A. (1991) Trishear fault-propagation folding. *Geology* **19**, 617–620.
Fischer, M. P., Woodward, N. B. and Mitchell, M. M. (1992) The kinematics of break-thrust folds. *Journal of Structural Geology* **14**, 451–460.
Freund, R. (1979) Progressive strain in beds of monoclinal flexures. *Geology* **7**, 269–271.
Hudleston, P. J. and Lan, L. (1994) Rheological controls on the shapes of single-layer folds. *Journal of Structural Geology* **16**, 1007–1021.
Jackson, M. D. and Pollard, D. D. (1990) Flexure and faulting of sedimentary host rocks during growth of igneous domes Henry Mountains, Utah. *Journal of Structural Geology* **12**, 185–206.
Jaeger, J. C. and Cook, N. G. W. (1979) Fundamentals of rock mechanics. *Chapman and Hall, London.*
James, A. I. and Watkinson, A. J. (1994) Initation of folding and boudinage in wrench shear and transpression. *Journal of Structural Geology* **16**, 883–893.
Jamison, W. R. (1987) Geometric analysis of fold development in overthrust terranes. *Journal of Structural Geology* **9**, 207–219.
Johnson, A. M. and Fletcher, R. C. (1994) *Folding of Viscous Layers.* Columbia University Press, New York.
Kattenhorn, S. A. (1994) Outcrop-scale fault-related folds, Valley and Ridge Province, Appalachians; comparison to kinematic model predictions. Unpublished M.Sc thesis, University of Akron.
Kattenhorn, S. A. and McConnell, D. A. (1994) Analysis of outcrop-scale fault-related folds, Eagle Rock, Virginia. *Southeastern Geology* **34**, 79–88.
Kilsdonk, B. and Fletcher, R. C. (1989) An analytical model of hanging-wall and footwall deformation at ramps on normal and thrust faults. *Tectonophysics* **163**, 153–168.
Klinger, R. E. and Rockwell, T. K. (1989) Flexural-slip folding along the eastern Elmore ranch fault in the superstition hills earthquake sequence of November 1987. *Bulletin of the Seismological Society of America* **79**, 297–303.
Koch, F. G., Johnson, A. M. and Pollard, D. D. (1981) Monoclinal bending of strata over laccolith intrusions. *Tectonophysics* **74**, T21–T31.
Lawn, B. 1993. *Fracture of Brittle Solids — Second Edition.* Cambridge University Press, New York.
Lewis, H. and Couples, G. D. (1993) Production evidence for geological heterogeneities in the Anschutz Ranch East Field, Western USA. In *Characterization of Fluivial and Aeolian Reservoirs*, eds C. P. North and D. J. Prosser, Special Publication of the Geological Society. 73, 321–338.
McMechan, M. E. and Thompson, R. I. (1989) Structural style and history of the Rocky Mountain fold and thrust belt. In *Western Canada Sedimentary Basin; A Case History*, ed. B. D. Ricketts, pp. 47–71. Canadian Society of Petroleum Geologists.
McTigue, D. F. and Mei, C. C. (1981) Gravity-induced stesses near topographys of small slope. *Journal of geophysical Research* **86**, 9268–9278.
Mitra, S. (1992) Balanced structural itnerpretations in fold and thrust belts. In *Structural Geology of Fold and Thrust Belts*, eds S. Mitra and G. W. Fisher, pp. 53–77. Johns Hopkins University Press, Baltimore, MD.
Mitra, S. and Islam, Q. T. (1994) Experimental (clay) models of inversion structures. *Tectonophysics* **230**, 211–222.
Mollema, P. (1994) The influence of structural position and lithology on the fracture distribution in the East Kaibab monocline, SE Utah: implications for fluid flow properties. Unpublished M.Sc. thesis, Stanford University.
Mosar, J. and Suppe, J. (1992) Role of shear in fault-propagation folding. In *Thrust Tectonics*, ed. K. R. McClay, pp. 123–132. Chapman and Hall, London.
Pfaff, V. J. and Johnson, A. M. (1989) Opposite senses of fold asymmetry. *Engineering Geology* **27**, 3–38.
Philip, H. and Meghraoui, M. (1983) Structural analysis and interpretation of the surface deformations of the El Asnam earthquake of October 10, 1980. *Tectonics* **2**, 17–49.
Price, R. A. and Mountjoy, E. W. (1970) Geologic structure of the Canadian Rocky Mountains between Bow and Athabasca rivers; a progress report. In *Structure of the Southern Canadian Cordillera*, ed. J. O. Wheeler, Vol. **6**, pp. 7–25. Special Publication of the Geological Association of Canada.
Ramsay, J. G. and Huber, M. I. (1987) *The Techniques of Modern Structural Geology; Volume 2; Folds and Fractures.* Academic Press, London.
Reches, Z. E. and Johnson, A. (1978) Development of monoclines: Part II. Theoretical analysis of monoclines. In *Laramide Folding Associated with Basement Block Faulting in the Western United States*, ed. V. I. Mathews, Geological Society of America, Memoir 151, pp. 273–311. Boulder.
Roth, W. H., Sweet, J. and Goodman, R. E. (1982) Numerical and physical modeling of flexure slip phenomena and potential for fault movement. *Rocks Mechanics Supplement* **12**, 27–46.
Scholz, C. H. (1990) *The Mechanics of Earthquakes and Faulting.* Cambridge University Press, New York.
Schultz, R. A. and Aydin, A. (1990) Formation of interior basins associated with curved faults in Alaska. *Tectonics* **9**, 1387–1407.
Suppe, J. (1983) Geometry and kinematics of fault-bend folding. *American Journal of Science* **283**, 648–721.
Suppe, J. (1985) *Principles of Structural Geology.* Prentice-Hall, Inc., Englewood Cliffs.
Suppe, J. and Medwedeff, D. (1990) Geometry and kinematics of fault-propagation folding. *Ecologae Geologicae Helvetiae* **83**, 409–454.
Tanner, P. W. G. (1989) The flexural-slip mechanism. *Journal of Structural Geology* **11**, 635–655.
Thomas, A. L. and Pollard, D. D. (1993) The geometry of échelon fractures in rock: implications from laboratory and numerical experiments. *Journal of Structural Geology* **15**, 323–334.
Timoshenko, S. P. and Goodier, J. N. (1934) *Theory of Elasticity.* McGraw-Hill, New York.
Watkinson, A. J. (1993) A footwall system of faults associated with a foreland thrust in Montana. *Journal of Structural Geology* **15**, 335–342.
Withjack, M. O., Olson, J. and Peterson, E. (1990) Experimental models of extensional forced folds. *American Association of Petroleum Geologists Bulletin* **74**, 1038–1054.
Yeats, R. S. (1986) Active faults related to folding. In *Studies in Geophysics*, ed. R. E. Wallace, pp. 63–79. National Academic Press, Washington, DC.
Zienkiewicz, O. C. and Taylor, R. L. (1989) *The Finite Element Method.* McGraw-Hill Book Company, London.

APPENDIX

Determining the normal stress tangential to frictional interfaces

Along a frictional interface the normal and shear stresses and displacements are calculated for the BEM solution. The normal stress tangential to the interface is not calculated but can be found from the normal stress and tangential displacement as described in Crouch and Starfield (1990, pp. 100–109).

Hooke's Law expresses the normal strain, ϵ_{xx}, in terms of normal stresses σ_{xx}, σ_{yy}, and σ_{zz} (Timoshenko and Goodier, 1934)

$$\epsilon_{xx} = \frac{1}{E}\left[\sigma_{xx} - \nu(\sigma_{yy} + \sigma_{zz})\right]. \tag{A1}$$

We assume that plane strain conditions dominate at depth within the Earth so that we only need to consider the stress state in the two-dimensional x–y plane. The normal stress, σ_{zz}, is related to σ_{xx} and σ_{yy} according to plane strain conditions (Timoshenko and Goodier, 1934)

$$\sigma_{zz} = \nu(\sigma_{xx} + \sigma_{yy}). \tag{A2}$$

Substituting equation (A2) in (A1) and rearranging (A1) allow us to express the normal stress, σ_{xx}, in terms of normal stress, σ_{yy}, and normal strain, ϵ_{xx}, as follows:

$$\sigma_{xx} = \frac{E}{1-\nu^2}\epsilon_{xx} + \frac{\nu}{1-\nu}\sigma_{yy}. \tag{A3}$$

In the case of a slipping interface, the normal stresses acting tangential to the interface are discontinuous across the interface and may have different values above and below the interface. We use a superscript to distinguish the upper (positive) and lower (negative) sides of the frictional interface. For the frictional interface sketch in Fig. 1 the normal tangential stresses are:

$$\sigma_{xx}^{+} = \frac{E}{1-\upsilon^2}\epsilon_{xx}^{+} + \frac{\nu}{1-\upsilon}\sigma_{yy}$$

$$\sigma_{xx}^{-} = \frac{E}{1-\upsilon^2}\epsilon_{xx}^{-} + \frac{\nu}{1-\upsilon}\sigma_{yy} \tag{A4}$$

The normal strain, ϵ_{xx}, equals the change in slip on the interface, $u_x(\epsilon_{xx} = \partial u_x/\partial x)$ (Timoshenko and Goodier, 1934). Where the tangential displacement is constant along the interface, the x-parallel strain is zero. Where the shear displacement, u_x, changes rapidly the x-parallel strain, ϵ_{xx}, will be concentrated

$$\sigma_{xx}^{\pm} = \frac{E}{1-\upsilon^2}\frac{\partial u_x^{\pm}}{\partial x} + \frac{\nu}{1-\upsilon}\sigma_{yy}. \tag{A5}$$

Using the backward difference method (Crouch and Starfield, 1990), the displacement gradient is determined at points between successive elements along the frictional interface (points A and B in Fig. 1). The interface normal, σ_{yy}, and shear, σ_{yx}, stresses are determined between neighboring elements by taking the average of the two elements. From the interface normal stress and the displacement gradients the tangential stresses above and below the interface can be determined between successive elements along the frictional interface.

Determining maximum principal stress and orientation

The maximum principal stress is calculated along the frictional interface at points between successive elements from the normal, shear and tangential stresses. The maximum principal stress is determined above and below the interfaces from the respective normal and shear stresses (Timoshenko and Goodier, 1934)

$$\sigma_1^{\pm} = \frac{\sigma_{xx}^{\pm} + \sigma_{yy}}{2} + \sqrt{\frac{(\sigma_{xx}^{\pm} - \sigma_{yy})^2}{4} + \sigma_{yx}^2}. \tag{A6}$$

If the maximum tensile stress exceeds the tensile strength of the rock a new fracture will grow perpendicular to the direction of maximum tension. The new splay crack is oriented at an angle α from the frictional interface that is $\pi/2$ from the orientation of the maximum tensile stress (Timoshenko and Goodier, 1934)

$$\alpha_1^{\pm} = \frac{\pi}{2} + \frac{1}{2}\tan^{-1}\left[\frac{2\sigma_{yx}}{\sigma_{xx}^{\pm} - \sigma_{yy}}\right]. \tag{A7}$$